

Fernow-510-c ✓

Accelerator Department
BROOKHAVEN NATIONAL LABORATORY
Associated Universities, Inc.
Upton, New York 11973

ISABELLE Project

Technical Note No. 320

(same as TLM - 23)

THE TWO LAYER ISABELLE CABLE MAGNET
DESCRIPTION AND TEST RESULTS

R.B. Palmer, J.G. Cottingham, R.C. Fernow, C.L. Goodzeit, E.R. Kelly,
M. Montag, J. Pasciak, S.D. Protopopescu, D.C. Rahm, W.B. Sampson,
R.P. Shutt, A.J. Stevens, I. Stumer and D. Tuttle

September 1981

Introduction

The philosophy behind the two layer magnet was to build it changing as little as possible from the standard ISABELLE $\cos\theta$ design but replacing the braid superconductor with Rutherford type cable. We believed that some of the more serious problems with the $\cos\theta$ magnet were due to inherent properties of the braid. The cable superconductor developed at Rutherford and used in FNAL magnets happens to be almost exactly half the width of the BNL braid so two layers of it would fit in the same radial space as in the braid magnet. The cable's properties are well understood and because of its narrower width the eddy currents induced during ramping are negligible. Also, because the amount of superconductor per unit volume is higher in the cable than in the braid we expect a two layer magnet to reach higher fields than the $\cos\theta$ magnets made with braid. Since FNAL magnets have smaller radii than the BNL magnets the regular FNAL cable is not keystoneed suitably for ISABELLE magnets. Luckily, a supply of surplus FNAL cable existed with almost optimum keystone and this made it possible to build test magnets without any long delays. A required modification from the standard design is the use of a split iron yoke. The cable is more compressible than the braid, and it is therefore impossible to apply sufficient coil prestress with a thermal insertion into a non-split yoke. We also believe the split yoke allows better dimensional control and other practical advantages, such as easy extraction of coils from yoke.

In the design, the basic coil shape of FNAL magnets was kept, but with some modifications to improve the uniformity of the field and thus increase aperture and reduce the load on the correction coils. Every effort was made

to match the dimensions of the standard $\cos\theta$ magnet, e.g., the inner and outer coil and the inner and outer iron yoke diameters are the same as before. This allowed the use of the present winding fixtures for making the coils and the existing fabricated components such as vacuum vessels, etc. In addition, the original concept for the correction coils can be used and the ISABELLE lattice remains unchanged.

In the following sections we describe details on the design of the two layer magnet, the superconducting cable, the mechanical construction and assembly procedures and the results of tests on the first two magnets. The results of the tests are very encouraging and indicate that the magnet may fulfill all expectations.

I. Conceptual Design

The cross section design started from a scaled up version of FNAL design (shown in Figure 1a). A problem with the FNAL cross section is that the higher order multipoles are much bigger than ISABELLE tolerances. The multipole coefficients are defined by a cylindrical harmonic expansion:

$$B_y(r, \theta) = B_0 \left(1 + \sum_{n=1}^{\infty} r^n (b_n \cos n\theta - a_n \sin n\theta) \right)$$

It follows that:

$$B_x(r, \theta) = B_0 \sum_{n=1}^{\infty} r^n (a_n \cos n\theta + b_n \sin n\theta)$$

where y and x are the vertical and horizontal coordinates respectively, r and θ the corresponding polar coordinates and the origin is at center of the magnet.

As a special case along the x axis the above become

$$B_y = B_o (1 + b_1 x + b_2 x^2 + \dots)$$

$$B_x = B_o (a_1 x + a_2 x^2 + \dots)$$

We will find it convenient later to use the quantities b' and a' which are defined as the contribution of each term to the field at 4.4 cm which is the radius of the beam tube (2/3 of the coil radius), i.e. the maximum possible working aperture of the magnets. Thus at $x = 4.4$ cm and $y = 0$:

$B_y = B_o (1 + b'_1 + b'_2 + \dots)$ and $B_x = B_o (a'_1 + a'_2 + \dots)$, by definition $b'_n = b_n (4.4)^n$ and $a'_n = a_n (4.4)^n$. These primed quantities give a better feeling for the contribution of each term to the field at the maximum aperture. By symmetry the design has all a's and all the odd b's equal to zero. Also b_2 and b_4 can be set to zero. However, b_6 and b_8 are then large: b_6 is ~ 36 times and b_8 is ~ 3 times the specified tolerances for ISABELLE. To correct this problem small wedges were added to both the outer and inner coils as shown in Figure 1b). A computer program was used to optimize the size of the blocks. The final configuration had negligible high order multipoles, a few percent of specified tolerances. By plotting the azimuthal distribution of the current integrated over intervals of 10° (Figure 2), one can immediately see that the final configuration (Figure 1b) is a fairly good approximation to a $\cos\theta$ distribution.

The cross section of the split iron yoke is shown in Figure 3. The saturation effects due to this yoke were studied using the program GFUN and were found to be acceptable, within an easily correctable range.

The design of the ends of the magnet is intrinsically a three dimensional problem. One can intuitively see what the end effects are by following the

contribution of one turn of cable to the current distribution as a function of the azimuth ϕ . Throughout most of its length it contributes at a fixed value of ϕ ; however, as it is wound around the end, there is an additional contribution at each ϕ all the way to the pole. The actual current distribution is shown schematically in Figure 4. One can see that as one adds many turns the extra contribution beyond that at fixed ϕ adds to the current near the poles and this tends to introduce negative multipoles. The effect can be corrected by inserting spacers between windings at the ends, thus increasing the contribution to the field integral from the turns near the midplane and decreasing that of the turns near the pole. A top projection of the ends for the outer and inner coils is shown in Figure 8. The configuration chosen keeps the multipoles well within tolerances. Another bonus from the spacers is to reduce the field enhancement near the ends. A current element at the end of the magnet will see contributions to the field coming from 3 sides (rather than 2) as cable is wound around it. Even with the end spacers there will be sections of cable at the ends that would see a larger field than anywhere else and this would lead to end quenching. To reduce the probability of end quenching the ends are taken outside the split iron yoke and instead, stainless steel end blocks are used to prevent any motion.

II. Superconducting Cable

For construction of the test magnets some relatively old (> 4 years) surplus superconducting cable from FNAL was available and happened to have almost the right dimensions for a ISABELLE type magnet. The cable is 0.307" wide and keystoneed .0525" thick on one side and .0465" thick on the other.

It is made of 23 strands of standard 2000 filament matrix superconductor with a ratio of 1.8 Cu to 1.0 NbTi. Each strand is nominally .027" in diameter. The cable used on CM1 and CM2 was measured to have a resistance at 10°K of 0.61 $\mu\Omega/cm$ or a resistivity ratio of about 50. Its critical current was 4600 Amps at 5.5 T and 4.22°K. The equivalent number for new cable is expected to be at least 5000 Amps. The cable is well insulated with two layers of 1 mil Kapton and one layer of 3 mil glass tape; this is sufficient insulation for at least 1000 volts turn to turn. In Figure 5 we show a cross section of the cable. The packing property is high (85% as compared, for example, to 73% for the braid). The mechanical properties of the cable were studied by applying pressure to little blocks 10 layers high and 3" long. Figure 6 shows the thickness variation as a function of pressure. After about 2 cycles the curve is reproducible. The Young's modulus obtained from the various test blocks varied between 1.5 and 2.0 x 10⁶ lbs-in⁻². Under final compression (\sim 10-11 Kpsi) the cable thickness is reduced by \sim 2%.

III. Magnet Description and Assembly

A vertical cross section of the half coils is shown in Figure 7. The outer radius is 3.23" and the inner one, 2.57". Each half coil is wound separately in an ISABELLE winding fixture with appropriate spacers for the inner and outer coils. The coils are cured in stages under pressure (4 Kpsi) at 157°C for three hours. The bonding between turns takes place with the epoxy on the glass tape just as in the braid cos θ magnet. Each coil has partial multiple cures, winding being stopped and the coil cured after placing the Cu wedge or an end spacer. Thus, there are 4 cures for the inner coil and 3 for the outer coil. Figure 8 shows a top view of the ends of both coils.

The end spacers on the first magnet were made from G10, in the second and subsequent magnets they are molded of epoxy resin (Araldite XD 580).

An insulating layer of 1 mil Kapton pressure sensitive tape is applied to the inner surface of the outer coil and a 2 mil layer of Teflon tape is applied to the outer surface of the inner coil and the outer surface of the inner coil. In CMI an additional 2 mil layer of Teflon tape was applied to the inside of the outer coil. The use of Teflon minimizes the stick-slip associated with the displacement of the coils relative to their bearing surfaces and makes it possible for the coils to be under almost uniform compression from the midplane to the pole. The entire coil package of the inner and outer coils, stainless steel posts and pole spacers and the necessary shims and insulation is shown in Figure 9. The insulation to ground is provided as follows:

a) Between outer and inner coil and the stainless steel posts and pole spacers, 0.200 G10 strips.

b) Between the outer surface of the inner coil and the stainless steel pole spacer, 3 layers of 0.010" G10 held together with 1 mil Mylar pressure sensitive tape.

c) At the outer surface of the outer coil one layer of 0.187" G10. This layer of G10 has cooling grooves in its inner side to permit helium flow. The grooves are 0.062" deep, 0.093" wide and are spaced 0.375" apart.

The coil assembly procedure starts with the placement of the stainless steel pole pieces and the outer G10 layers in the iron yoke. The pole pieces are set in a fixed location in the yoke with a key. Solder joints are made between the inner and outer coils (7 1/2" long). Then the bottom coils are laid into the pole spacer and shimming is added if necessary. The same

procedure is followed for the top coils. When the top half is assembled a special expandable mandrel is installed, the whole upper assembly is turned over and then lowered over the bottom half. Before bolting the two halves of the iron yoke, the mandrel is expanded applying a light outward pressure on the coils. This ensures that the coils remain in contact with the yoke at the initial stage. When the gap between the yoke halves is less than 60 mils, the mandrel is collapsed and removed. The iron yoke is then bolted to apply a compressive prestress $\sim 11 + 1$ Kpsi on both inner and outer coils at room temperature. When cooled to 4°K the prestress is reduced by about 3 Kpsi. This amount of prestress is calculated so that the polar regions of the coils remain under compression at fields up to 6.5 T.

The iron yoke from CM1 and CM2 is made of 6" blocks of epoxy-glued iron laminations (Figure 10 shows one lamination). Each block has two 13/16 vertical holes bored on each side for 3/4" stainless steel bolts. Stainless steel rails (5/8" thick) are used to join the blocks longitudinally, keeping a 1/16" gap between blocks. This method of construction is used to approximately match the thermal contraction of the yoke to that of the coil. The stainless steel rails shrink more than the iron. So, as the magnet is cooled, the gap between the blocks decreases and no longitudinal stresses build up in the coil. Every other block has a built-in jack to allow the top block to be lifted for any minor adjustments. The last 3" of the coils at both ends are outside the iron core, as we indicated previously, to reduce the field enhancement at high fields. The coil ends are held in 8" stainless steel blocks joined to the iron yoke via the stainless steel rails. The coils are also restrained longitudinally by end plates to prevent any longitudinal

motion of the coils with respect to the iron yoke when the magnet is energized. A partial view of the core assembly is shown in Figure 1.

After the magnet is assembled a bore tube is inserted (but before the magnet is fully closed). The outer surface of this tube is helically grooved to permit He flow along the inside of the inner coil. Note that the inside coil is cooled by the flow at the inner surface and the outside coils at the outer surface; there is no other flow between the two coils. The bore tube fits snugly only at the ends so that elsewhere there are no forces between it and the magnet itself. In the second magnet the bore tube contained a sextupole coil. Future magnets will also have octupole and decapole corrections.

The first magnet built (CM1) was 72" long and was finished six months after design was started (seven months after it was approved for construction). It was assembled and ready for tests only three days behind schedule. The second set of coils (CM2) was ready four weeks later.

IV. Tests of 72" Magnets (CM1 and CM2)

The first magnet (CM1) was first checked at room temperature for shorts and none was found. The turn-to-turn insulation was good up to at least 1 Kv, coil-to-coil insulation ≥ 3 Kv and coil-to-ground, ≥ 5 Kv.

The magnet was then inserted in a regular test Dewar, cooled to 4.5°K and ramped at 8 A/sec. The first quench occurred at 4120 A, corresponding to a field of 5.35 T. All subsequent quenches at the same temperature occurred at about the same value, i.e., the magnet exhibited no training, a rather remarkable performance. A plot of quench number vs. field is shown in

Figure 12a). Most of the points are at 4.5°K and cluster around 5.35 T. A few points were taken at 4.8° K, those quenches cluster around 5.1 T and a few others at 3.7-3.8° K which cluster around 5.85 T. The magnet therefore behaved as if it had reached the "short sample limit." To see if this is indeed the case one has to compare the maximum field reached with the measured short sample limit. The short sample limit was measured to be I_Q (quench current) = 4600 A at 4.22° K and 5.5 T. In order to compare this value with the magnet behavior one needs to correct for a 2% field enhancement, for I_Q dependence on B and for temperature dependence. For this calculation one makes the assumption that $B * I \sim \text{constant}$. On Figure 13 we show data points taken for I_Q as function of temperature at a given field and the extrapolated points for the two layer magnet. On Figure 14 we plot the measured load line (i.e., field vs. current) for the CMI magnet and the predicted quench current vs. field for 4.8° K, 4.5° K, 4.22° K and 3.8° K. Figure 15a) shows the observed magnet performance and the predicted short sample limit with $\pm 2\%$ error. The points clearly show that the magnet is quenching at the expected limit and proves that the magnet limitations are not due to any mechanical effects but purely to properties of the superconducting cable itself. This gives us hope that with the more recent cable used at FNAL, with a typical $I_Q = 5120$ at 4.22° K and 5.5 T (measured at BNL), we can expect to achieve fields as high as 6.2 T at 3.8° K.

The same testing sequence was followed on CM2. In this magnet the bore tube had a sextupole correction coil. When first assembled, two turn-to-turn shorts were found. It was suspected (but not proven) that the diameter at the ends of the bore tube was too large, thus applying strong radial pressure

on the coils. The magnet was dismantled, the bore tube ground down to reduce its diameter by a few mils, various small defects corrected, and then reassembled. Shorts did not come back at this point. It was then inserted into the Dewar, cooled to 4.5°K and ramped at 8 A/sec. The first quench occurred at 4050 Amps (corresponding to 5.05 T) and all subsequent ones at 5.35 T (same as C11). The quench number vs. field is shown in Figure 12b) and in Figure 15b) the observed magnet performance and the predicted short sample limit. Just as C11, C12 is quenching at the expected limit.

Before the magnets were cooled the field components were measured with a 10 A current. The measurement errors at this current are too large for the higher harmonics; the low harmonics agreed with the later cold measurements. It seems therefore possible that with higher currents and better measurements the magnet field quality may be checked before cool-down. Because the surplus cable thickness varied $\sim \pm 1$ mil in 60 mils one could not really attempt to meet design specifications (on one layer of C11 one turn even had to be left out). Therefore, the magnet was shimmed to obtain the correct prestress and then the field multipoles were calculated based on the size of the shims. The actual coil positions were not measured, only the known shim sizes were used to predict the multipole components. In Table I we compare the b' and a' values and the actual measurements at 1200 Amps for both C11 and C12 (i.e., well before saturation). The agreement is generally good except for a'_1 and a'_3 , particularly the latter which is more than 4 times BNL tolerance. The fact that the a 's are not zero indicates that we are not able to make the top and bottom half of the magnet identical. The fact that some are not even within the predictions indicates that we have not yet learned how to measure this mismatch. We believe these problems should be solved when better cable

is used. Its thickness is now controlled 4 times better than the surplus cable used for CMI and CM2.

In these magnets there are basically no effects on the multipoles during ramping, a.c. and d.c. multipoles are the same within measurement errors up to ramp rates of 120 A/sec. The difference between cable and braid to first order reflects basically the difference in the width, the cable is only half as wide and the eddy currents go roughly like the width to the 5th power.[†] When the magnet is ramped at high rates (> 40 Amps/sec) it seems to reach slightly higher fields before quenching than at lower ramp rates. It has been demonstrated on CM2 that this is due mostly to a delay between the time when the quench current is reached and the time when the quench actually starts. When the ramping at high rate is stopped at a quench current obtained at low rate the magnet quenches a second or two later.

The magnetization effects were studied for CMI by ramping the magnet up and down at 4.5°K and at 3.8°K, b_2' vs. current is shown in Figure 16, $\Delta b_2'$ at injection is 11.2×10^{-4} (tolerance $\sim 1.4 \times 10^{-4}$), close to the predicted value 10.2×10^{-4} . The fluctuation from magnet to magnet (based on experience at FNAL) are expected to be ~ 0.3 of BNL tolerance, so pose no serious problems. Furthermore, the temperature effect from Figure 16 implies that to meet BNL tolerances the random temperature variations must be controlled to 0.7°K. This should not be a problem.

The saturation effects at 5 T are 20% worse on the cable magnet than on the standard $\cos\theta$ design (11% vs. 8.5%) because of cutouts, stainless steel

[†]The eddy currents actually go like $\propto w^3 t^2$ where w is the width and t the transposition length. If everything scaled equally the effect would be like w^5 . In fact t for the cable is 1/4 that of the braid so that the eddy currents are ~ 100 times smaller for equal interstrand resistivities.

bolts and cracks between 6" blocks of the iron yoke. Saturation as a function of field is shown in Figure 17, this is not a problem at 5 T, but by 6 T, the amount of stray field is probably unacceptable. If one wanted to push this magnet as high as 6 T (possible with better superconductor) the amount of iron will have to be increased. Because of saturation effects the multipoles change as a function of current. Figure 18 shows b_2' and b_4' as a function of current measured in CML. The overall excursion from injection to maximum is 27×10^{-4} for b_2' and 2.6×10^{-4} for b_4' . This should not be difficult to correct.

The first magnet was also tested for quench protection. All quenches in the self protection study originated in the inner coil. The value of $\int I^2 dt$ was measured as a function of the external protection resistance R_{ext} (for $I = 4200$ Amps). The results are shown in Table II together with predicted values. The integral $\int I^2 dt$ can be related to the maximum possible temperature (T_{max}) during a quench. To obtain T_{max} for the cable one can use the $\int I^2 dt$ vs. T_{max} relation which is known for the braid and scale it using resistance measurements. This method agrees within 10% with published FNAL data. The danger point for the cable is 7.0×10^6 amp² sec, corresponding to $T_{max} = 450^\circ$ K. In addition to $\int I^2 dt$ other quantities that were determined were the quench velocity, ~ 1.7 msec/turn (assuming the quench to have originated near the end of the coil), the time taken for the quench to propagate from the inner coil to the outer coil ~ 53 msec and the time taken for the quench to propagate to the opposite half coil ~ 100 msec. It is with the use of these numbers and a program originally designed to calculate $\int I^2 dt$ for the braid magnets that the predicted values in Table II were obtained.

This program can be used to predict $\int I^2 dt$ for a long ISABELLE size magnet (x3). One obtains at $I = 4200$ A $\int I^2 dt = 5.9 \times 10^6$ A² sec. This may seem uncomfortably close to 7×10^6 A² sec; however, it corresponds to $M = 301^\circ\text{K}$ (21°C) quite far from $T_{\text{max}} = 450^\circ\text{K}$ (170°C). It is possible than, that the long cable magnets will be self-protected, at least at $I = 4200$ A.

At low currents it takes a longer time for a quench to propagate, so $\int I^2 dt$ can be higher. To study $\int I^2 dt$ as a function of current, a heater was inserted in CM2 during assembly. With this heater it was possible to induce quenches at low currents. The worst case $\int I^2 dt$ was found to be 5.3×10^6 A² sec at 2500 A. Whether this implies that at some current the long magnets may reach the danger point still needs some study. Using an external power supply three quenches were generated at 2500 A with $\int I^2 dt = 5.9 \times 10^6$ A² sec. No deterioration in magnet performance was observed after these quenches. The next magnet CM3, will have several heaters so that $\int I^2 dt$ can be studied as a function of both current and quench location. It will also be tested in both liquid and super-critical He. Azimuthal propagation is expected to be better in the latter.

The sextupole trim coil was tested with CM2. It in no way affected the performance of CM2 when powered. The coil needs to work in the range ± 130 A. It was run repeatedly at ± 100 A and once at ± 200 A (at 5 T). No quenching occurred. It was also powered during ramping in the mode needed for correcting saturation effects. The b_2 was kept within tolerance without difficulty throughout. The trim coil affects also b_4 but the change is well within tolerance after the magnet is cycled.

V. Conclusions

The first magnets built and tested (CM1 and CM2) fulfilled expectations beyond what anyone hoped. CM1 reached maximum field B_{\max} on the first quench and CM2 on the second quench. B_{\max} was a function of temperature, just as expected if the cable had reached its "short sample" limit. They had no detectable eddy currents up to ramp rates of 120 A/sec. The magnet seems to have quench self-protection but at some currents the margin may be uncomfortably small, so a protection scheme will be incorporated. Their field quality, although not within ISABELLE specifications, is reasonably well understood. There is high hope that if cable currently manufactured (instead of 4 years old surplus stock) is used the field quality requirements will be met. In addition to replacing braid by cable there are many mechanical differences between this design and the $\cos\theta$ magnet, the most significant being the use of a split iron yoke made of blocks, restraining the ends with stainless steel instead of iron, and providing non stick-slip bearing surfaces. Whether any one or all of these differences are responsible for its better training characteristics may be worth investigating to achieve an optimum cost for production models. However, the present design performs very well and the main task ahead is to verify that a magnet three times as long will be able to repeat its performance. Since the magnet ends represent the most difficult part of the magnet assembly (and will remain unchanged), we believe the increase in length should not be a factor affecting the performance. Thus, we feel confident that the long magnets will do as well.

Acknowledgements:

We wish to thank the technicians in the ISABELLE and Physics Department who did an outstanding job in the making and assembly of these magnets:

Ray Cerutti, Joe Cracco, Roger Davis, John Donnelly, Gene Hassell, Augie Hoffmann, Helen La Sauce, Bill Lenz, Jerry Mayman, Vinnie Mirizio, Erno Ostheimer, Al Roberts, Joe Russo, Joe Scheliga and Mona Vitale, and also the designers: Bill Dieffenbach and Sal Morano. The Physics Shops under the direction of Al Roebuck and the Central Shops under the direction of Bob Lehn exerted themselves to ensure that all the pieces were ready on time. We also wish to thank the MIT Magnet Lab machine shop for their great help. We thank the Magnet Division at ISABELLE, directed by R.R. Rau, who provided us with valuable technical help and advice and with the winding fixtures for the coils. The magnet measurement group under R. Engelmann and K. Jaeger did a superb job in testing CM1 and CM2. Finally we wish to thank N. P. Samios for his constant support and encouragement.

Table I

Calculated and Measured Multipoles for CM1 and CM2

| Coefficient | $\times 10^{-4}$ | | | | | | |
|-------------|------------------|------------|----------|---------------------|------------|----------|---------------------|
| | CM1 | | | CM2 | | | |
| | Tolerance | Calculated | Measured | Δ/TOL | Calculated | Measured | Δ/TOL |
| b_1^1 | 3.1 | 0.0 | 0.9 | 0.3 | - .09 | 0.26 | 0.1 |
| b_2^2 | 1.3 | -13 | -12 | 0.8 | 1.6 | 8.7 | 5.2 |
| b_3^3 | 1.0 | 0.0 | 0.0 | 0.0 | - 0.1 | 0.0 | 0.1 |
| b_4^4 | 0.75 | - 9.4 | - 9.9 | 0.7 | - 3.5 | - 4.3 | 1.1 |
| b_5^5 | 0.53 | 0.0 | 0.04 | 0.1 | - 0.01 | - 0.1 | 0.2 |
| a_1^1 | 3.1 | - 2.2 | 4.4 | 2.1 | 45.3 | 41.8 | 1.1 |
| a_2^2 | 1.3 | 0.56 | - 0.56 | 0.9 | - .04 | - 0.56 | 0.4 |
| a_3^3 | 1.0 | - 2.2 | - 6.6 | 4.4 | 1.6 | - 5.1 | 6.7 |
| a_4^4 | 0.75 | - .07 | - 0.14 | 0.1 | 0.0 | - 0.94 | 0.8 |
| a_5^5 | 0.53 | 0.60 | 0.68 | 0.2 | - 1.7 | - 1.7 | 0.0 |

Table II

| R_{ext} (m Ω) | $\int I^2 dt$ vs. R_{ext} for CMI | | |
|-----------------------------------|--|----------|---------------------------------|
| | $\int I^2 dt$ (10^6 Amps sec) | | |
| | Calculated | Measured | T_{max} (Estimated) |
| 60 | 3.6 | 3.8 | 150 $^{\circ}$ K |
| 35 | 4.1 | 4.1 | 165 $^{\circ}$ K |
| 10 | 4.5 | 4.2 | 170 $^{\circ}$ K |

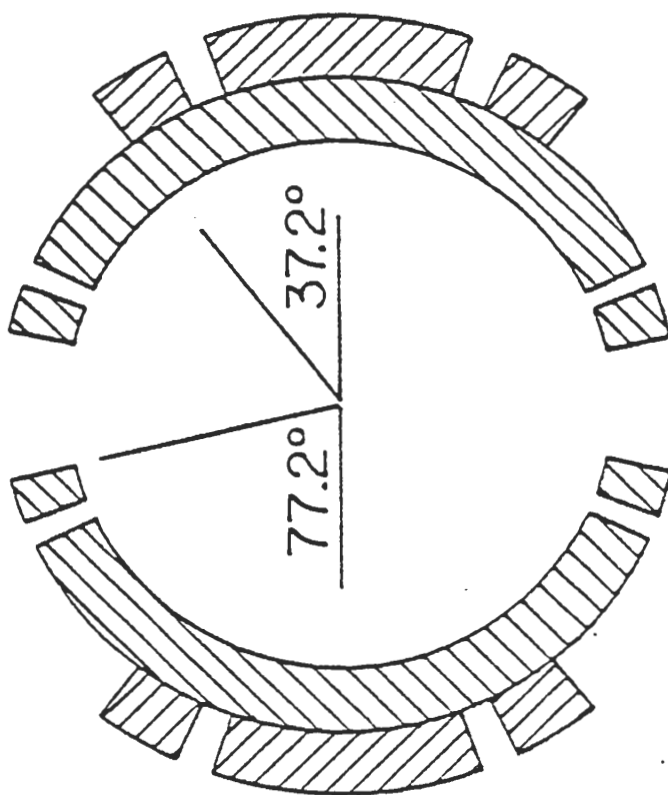
Figure Captions

- Figure 1 Cross section of two layer magnet designs: (a) Fermilab design, (b) Present ISA design.
- Figure 2 Current distribution integrated in intervals of 10° as a function of azimuth ϕ ($\phi = 0^\circ$ at the median plane, 90° at the pole).
- Figure 3 Cross section of iron yoke in present ISA design, bolts are of stainless steel.
- Figure 4 Current distribution for one turn integrated over length for a small ϕ interval as a function of the azimuth ϕ ($\phi = 90^\circ$ at the pole).
- Figure 5 Cross section of the superconducting cable showing schematically typical strand distortion. Before compression into the cable strands are nominally .027" in diameter.
- Figure 6 Variation under pressure of a 3" long, 10 layers high, stack of superconducting cable. After two cycles the variation is reproducible.
- Figure 7 Cross section of outer and inner coil.
- Figure 8 Rolled out top view of coil ends (a) inner coil, (b) outer coil.
- Figure 9 Cross section of a fully assembled magnet (excepting yoke).
- Figure 10 Front view of one lamination for the iron yoke.
- Figure 11 Partial view of a closed yoke with stainless steel end.
- Figure 12 Quench field vs. quench number (a) CM1, (b) CM2.
- Figure 13 Measured points of quench current vs. temperature at various fields for a short sample. The open circles are points extrapolated from the data.

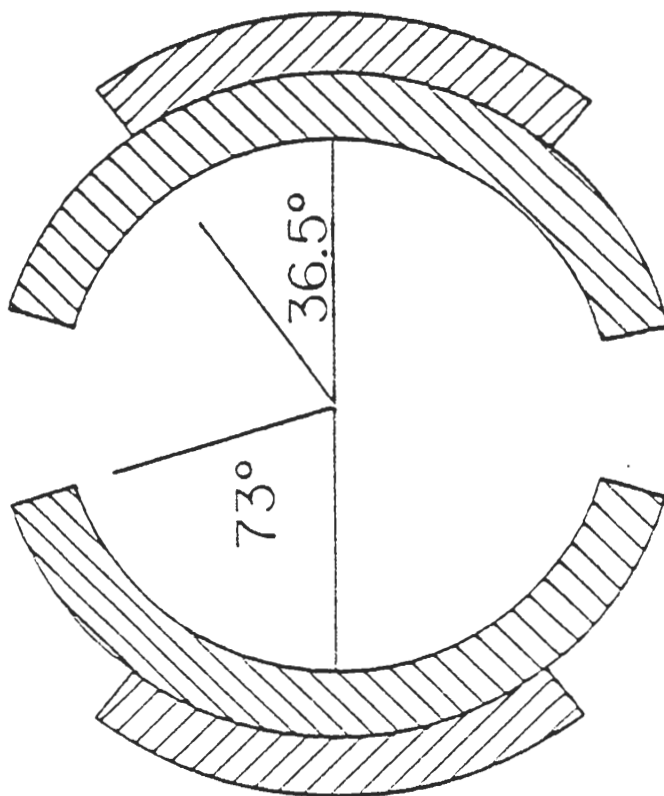
Figure Captions (continued)

- Figure 14 Load lines calculated for CMI magnet, dashed line is the one expected without iron saturation, solid line is the one with the saturation of present yoke. Points are the predicted quench currents (and field) for a given temperature.
- Figure 15 Quench field vs. temperature (a) CMI, (b) CM2. The dashed lines give the expected range calculated from "short sample limit" measurements.
- Figure 16 b_2' vs. current at 4.5°K and 3.8°K . The lower curves are for increasing currents and the upper curves for decreasing currents.
- Figure 17 Calculated magnet saturation as a function of the magnetic field. The upper curve is for the braid magnet, the lower curve, for CMI.
- Figure 18 b_2' and b_4' vs. current for CMI.

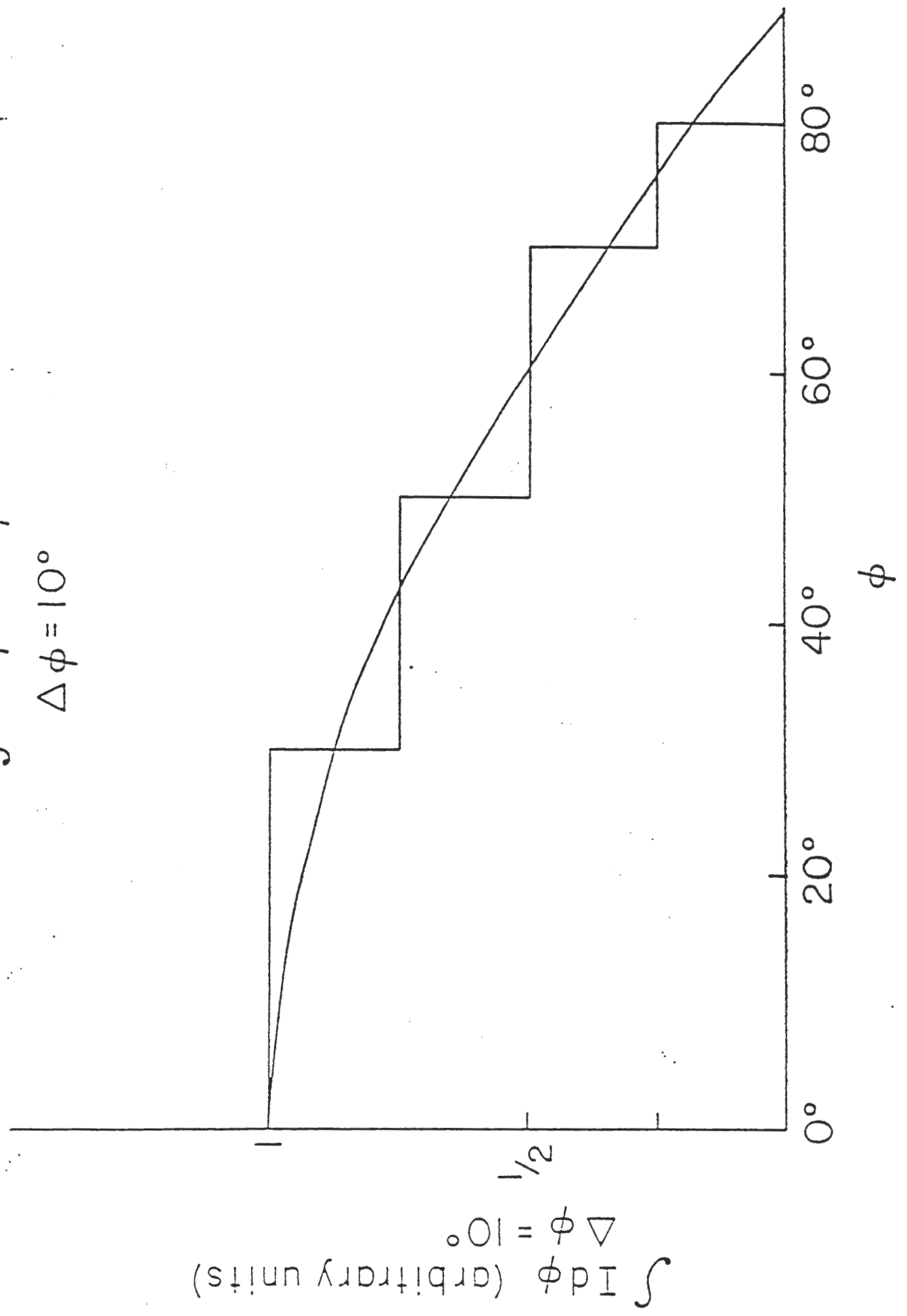
(b)



(a)



$\int I d\phi$ vs. ϕ
 $\Delta\phi = 10^\circ$



$\int I d\phi$ (arbitrary units)
 $\Delta\phi = 10^\circ$

Figure 2

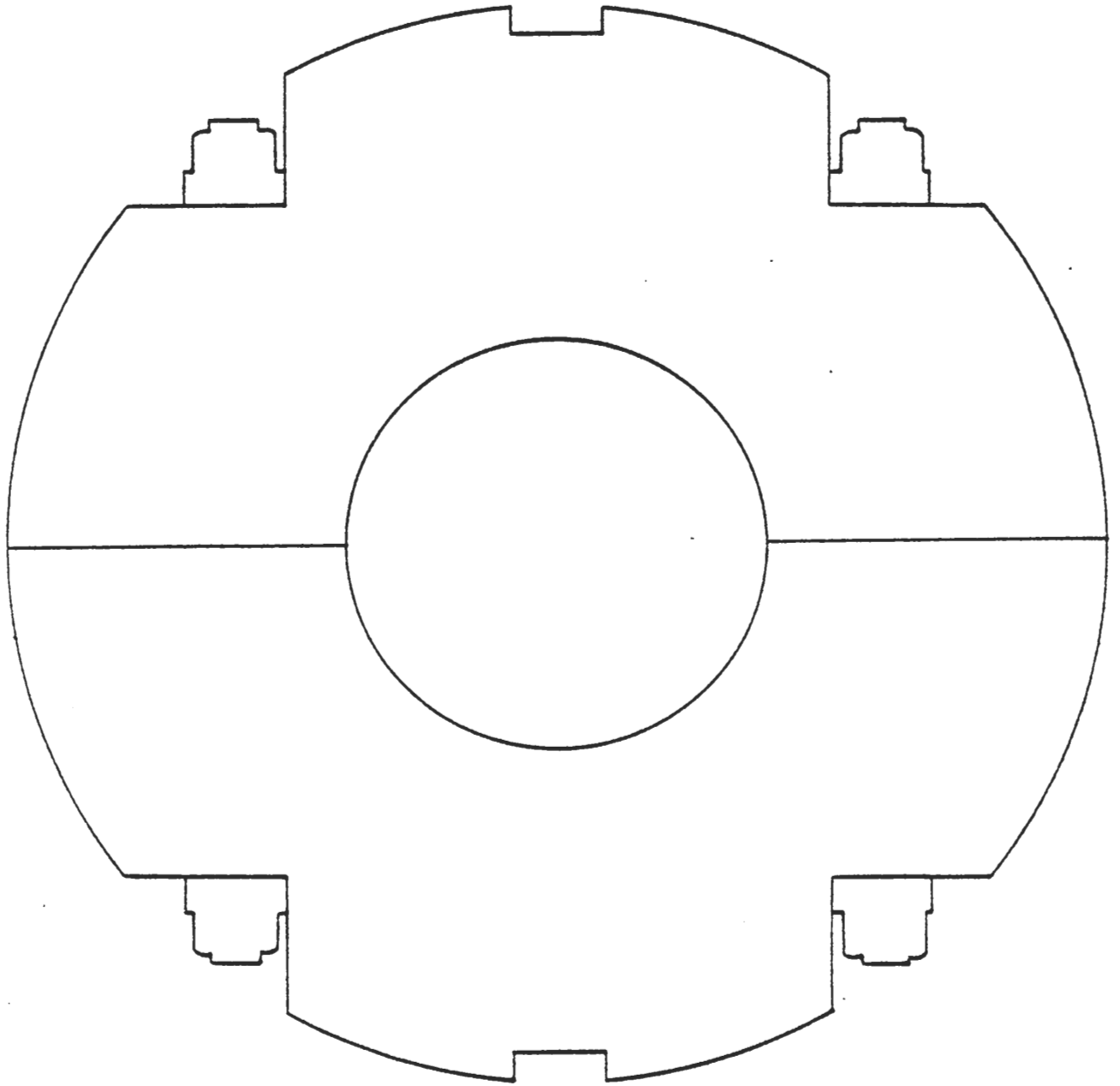


Figure 3

$\int I_{d\ell}$ VS ϕ FOR ONE TURN (AT 20°)

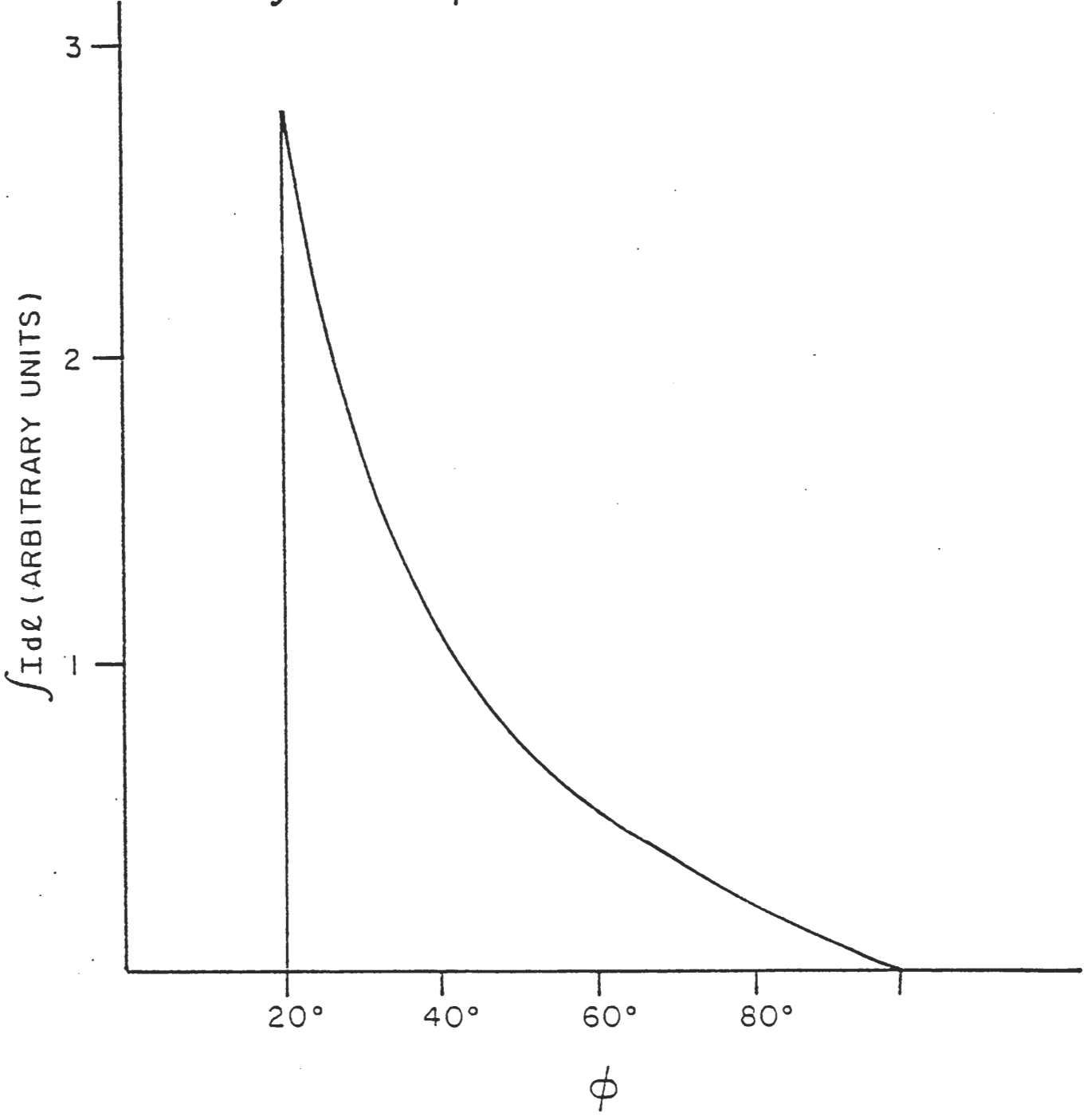


Figure 4

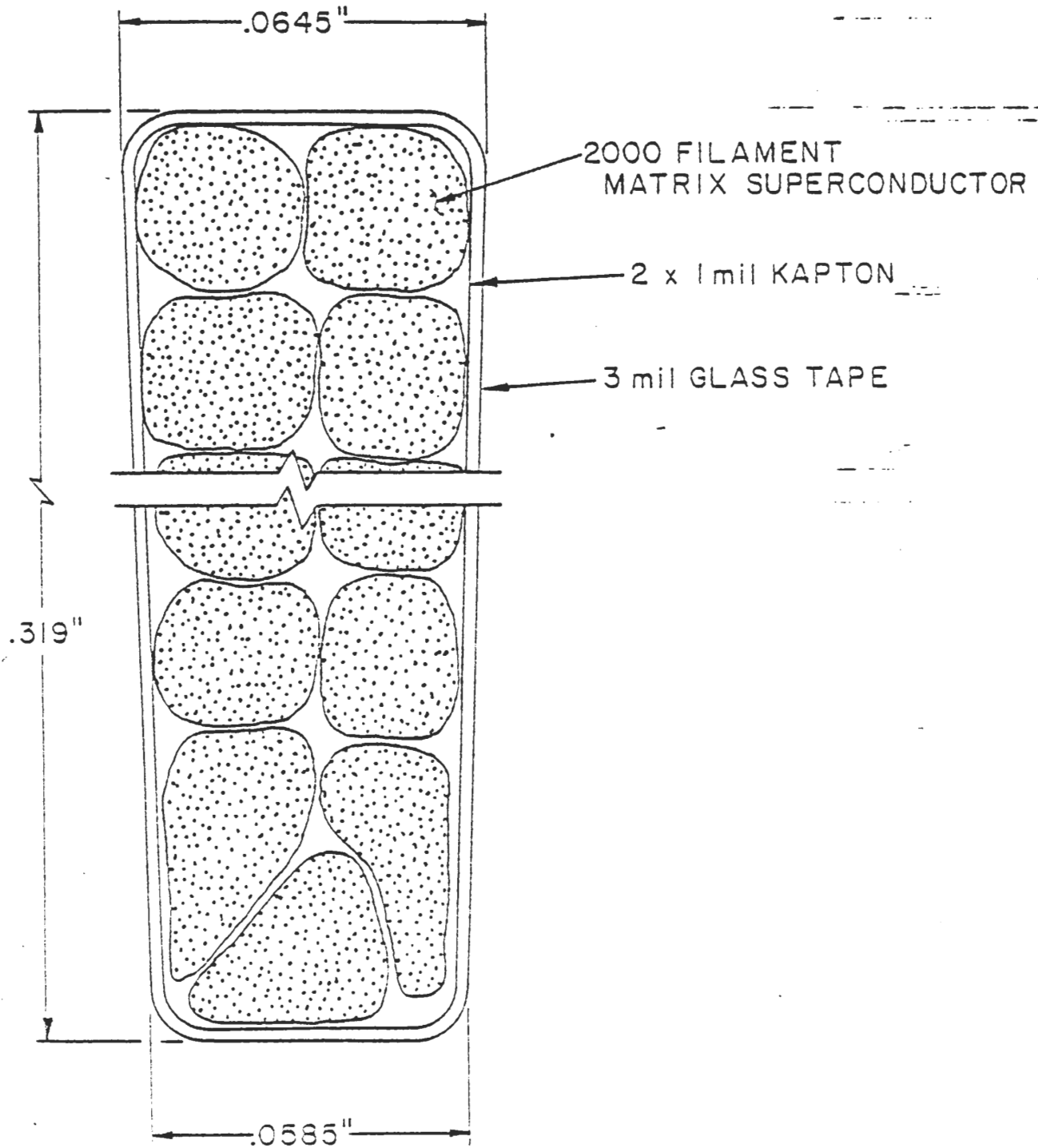


Figure 5

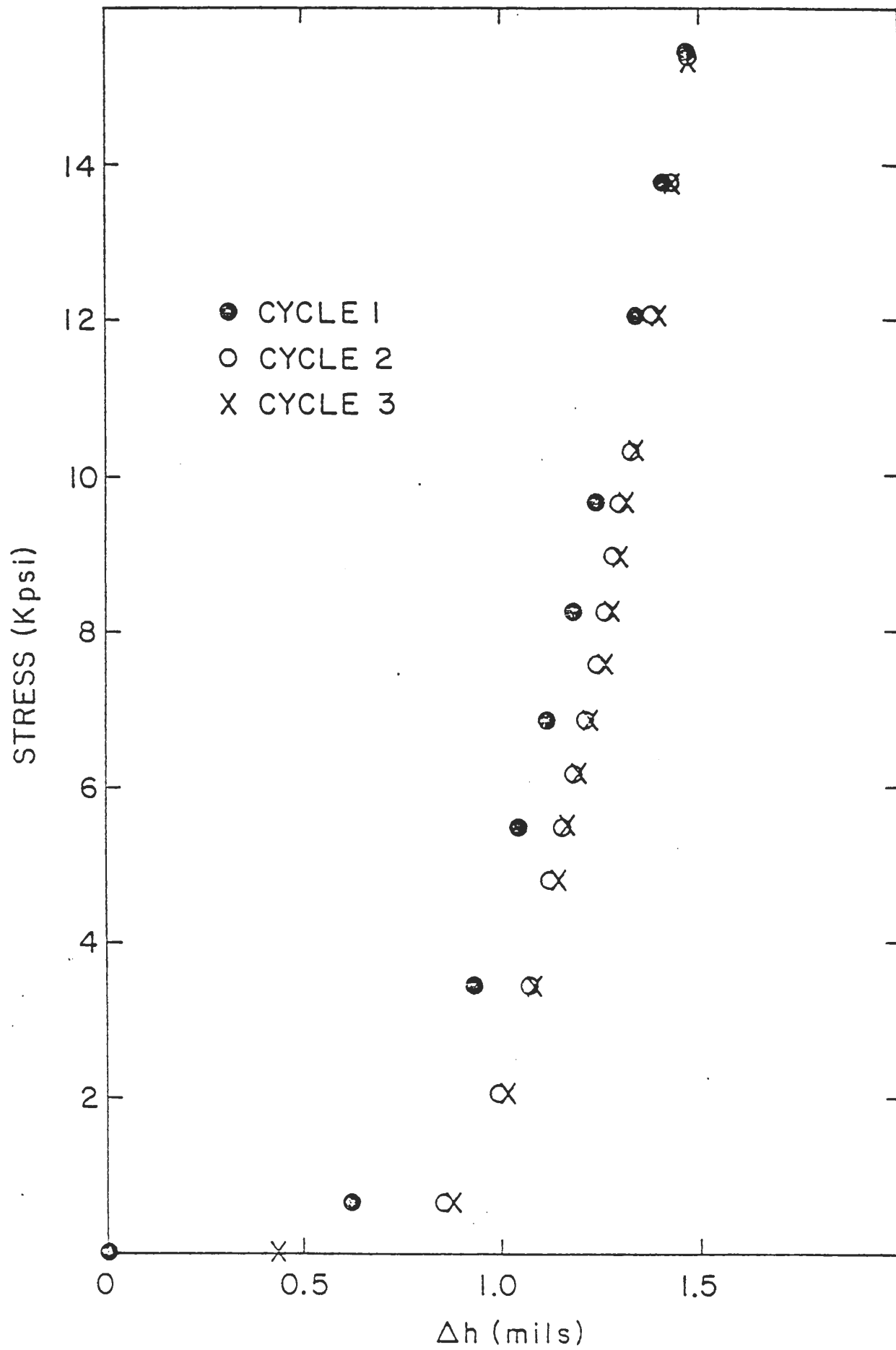


Figure 6

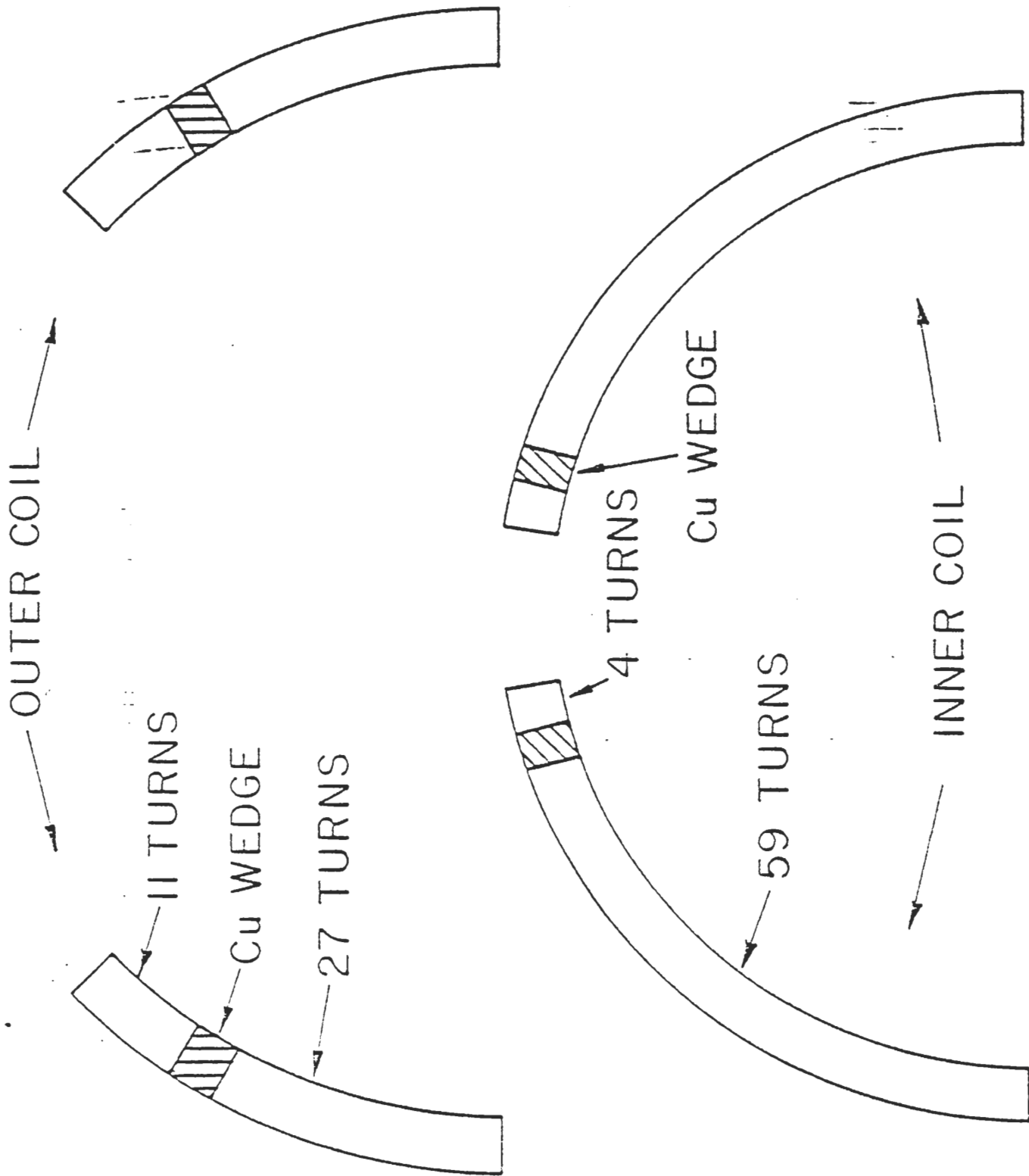


Figure 7

SPACERS & END PIECE - INNER COIL

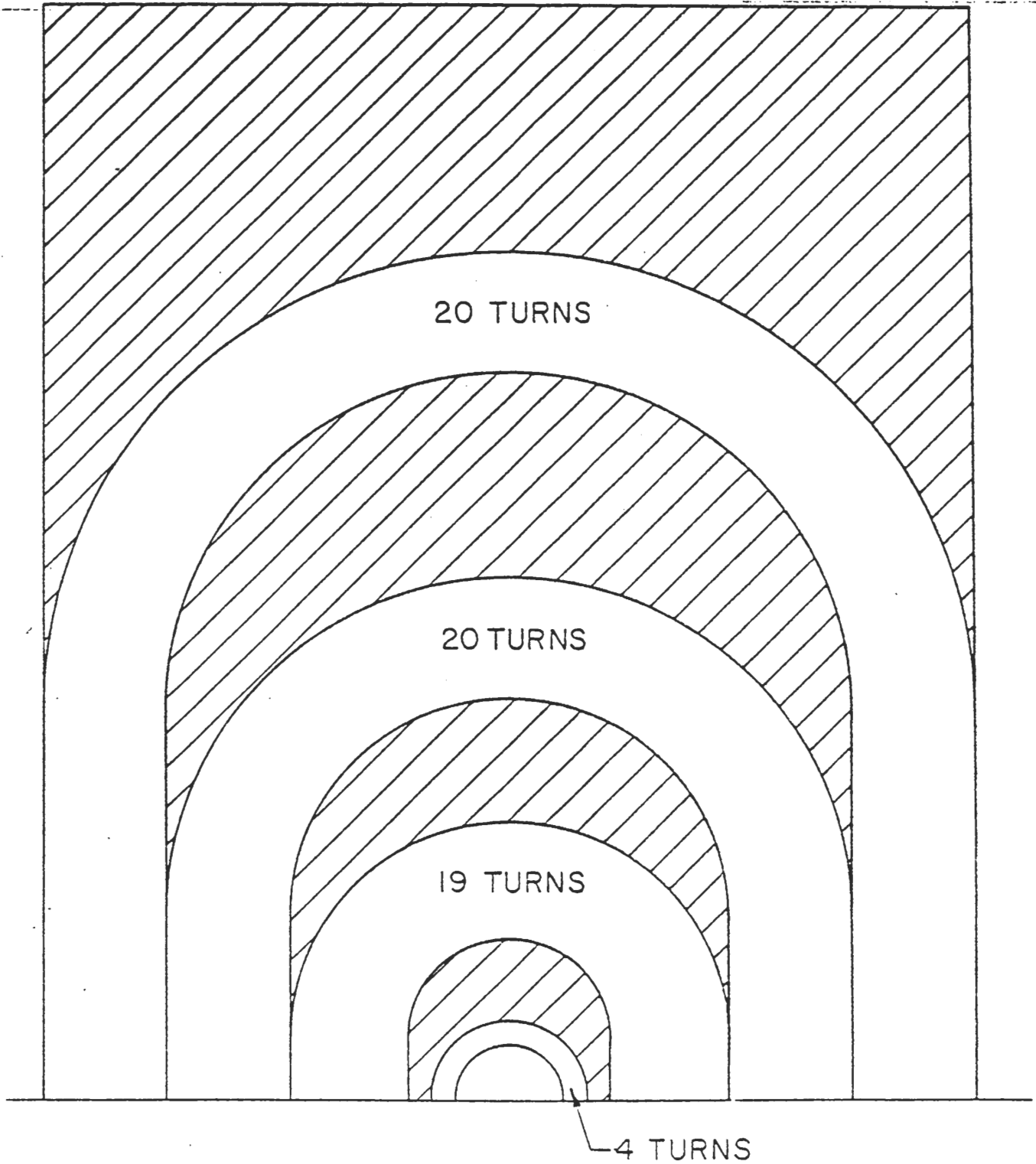
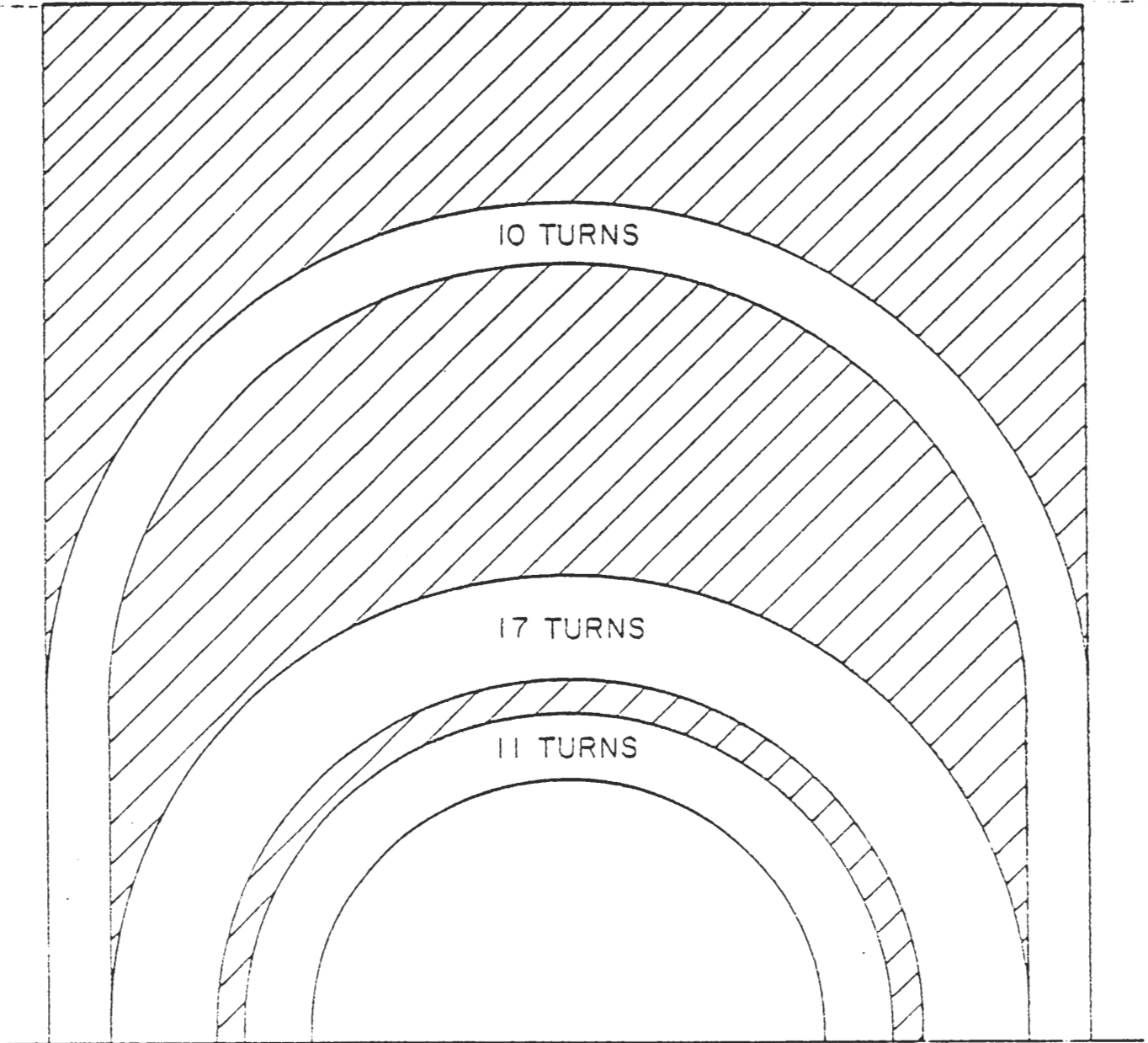


Figure Sa

SPACERS & END PIECE - OUTER COIL



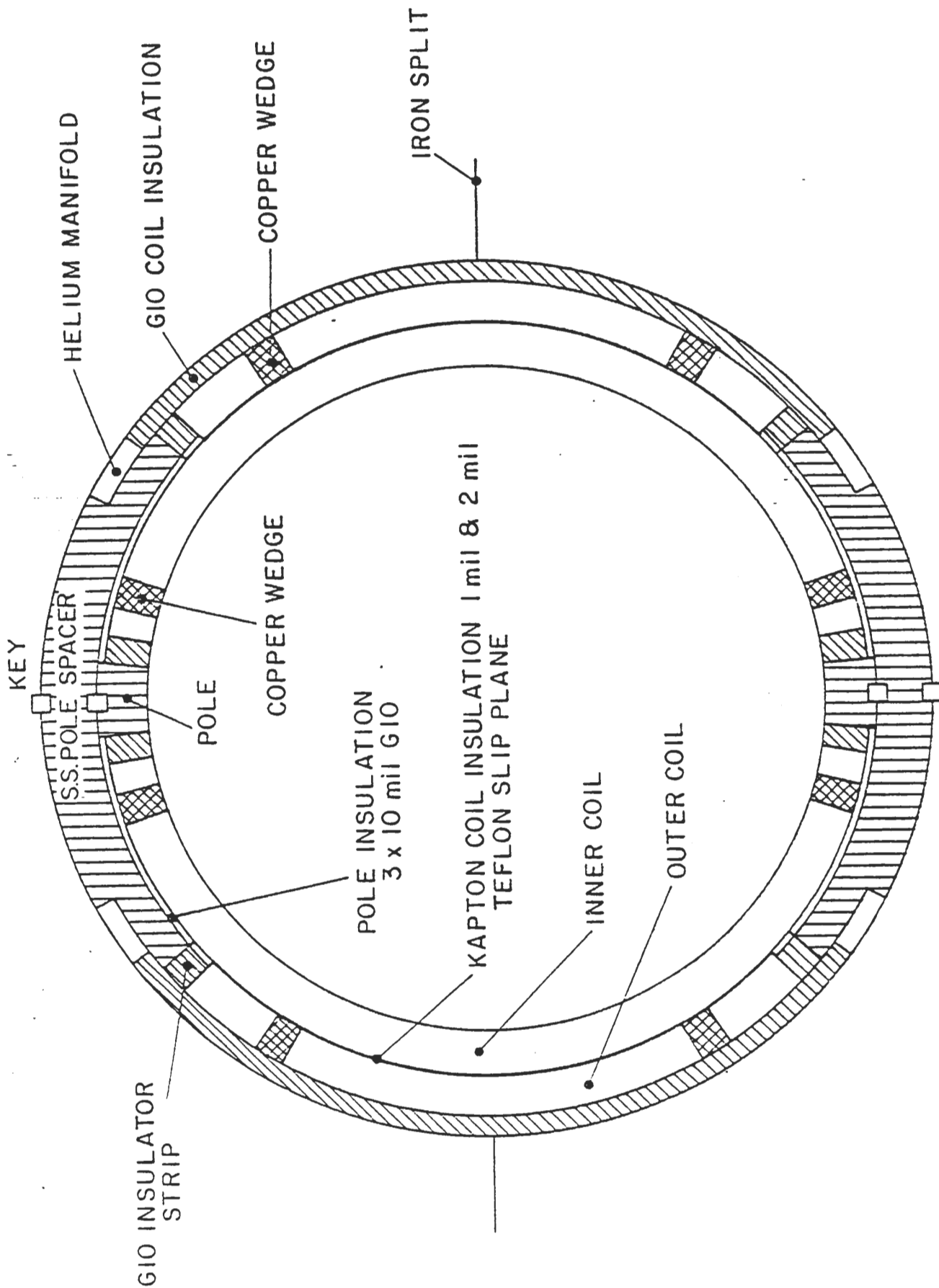


Figure 9

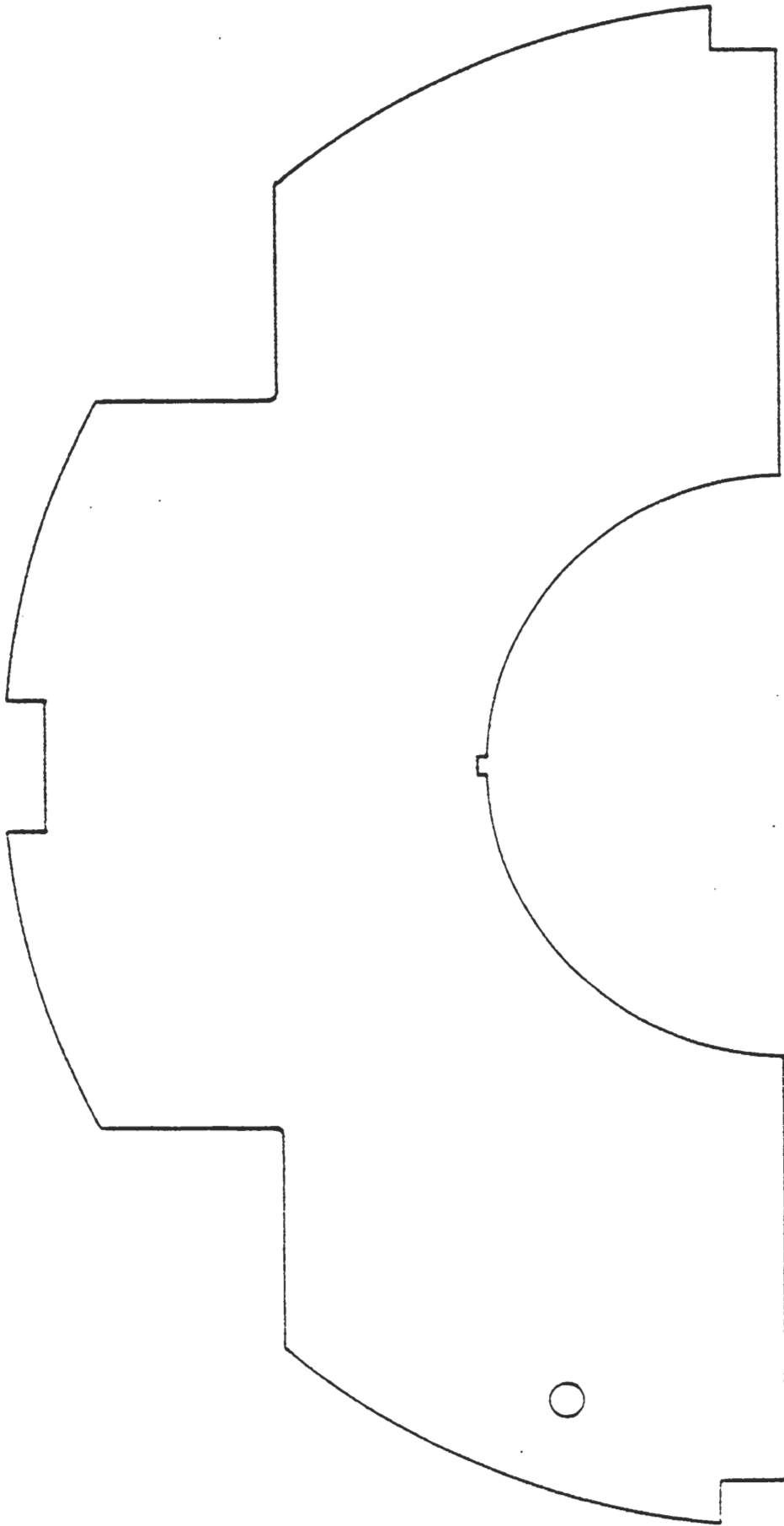
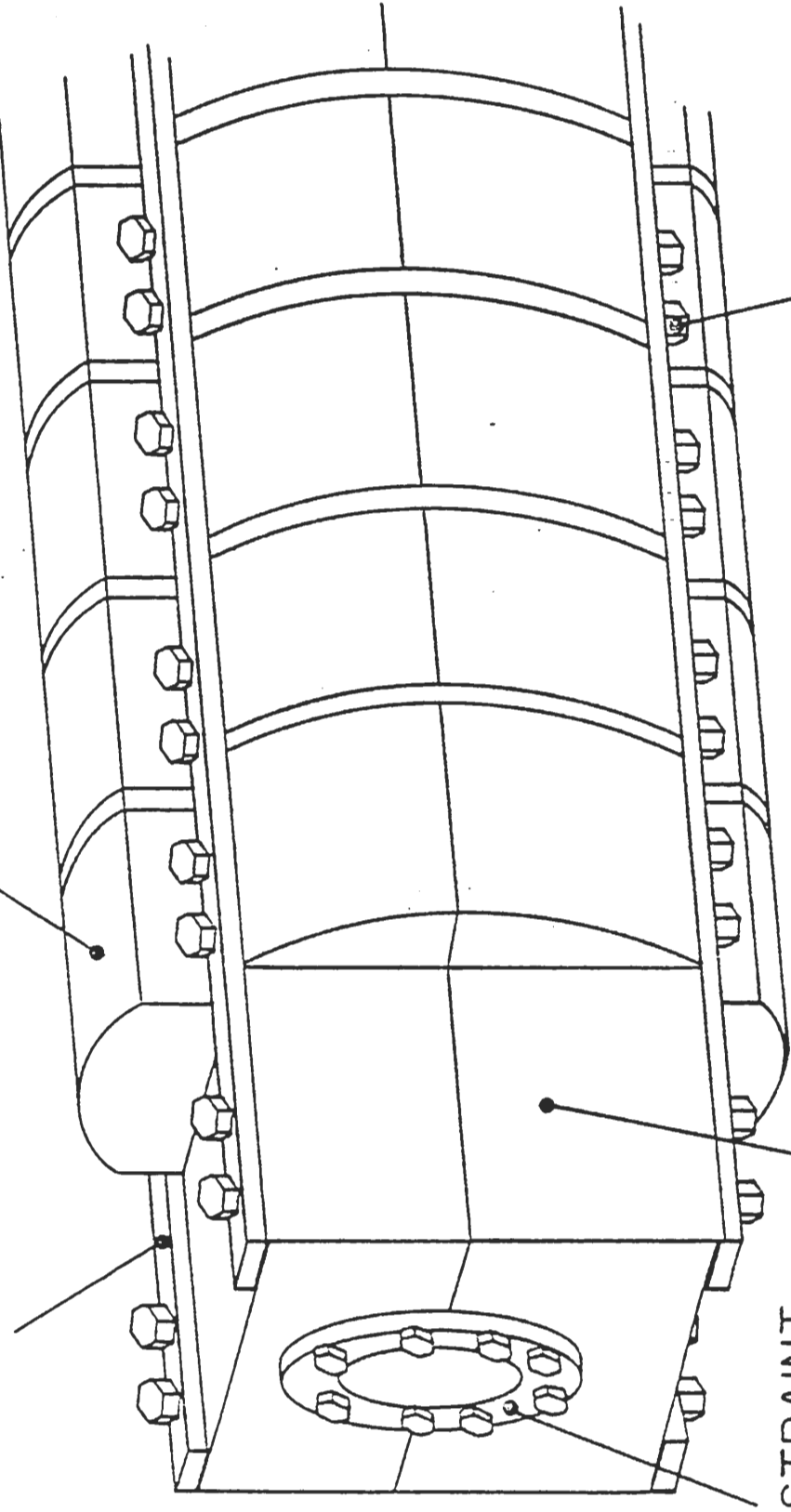


Figure 10

BLOCKS MADE OF GLUED LAMINATIONS

STAINLESS RAIL



END CONSTRAINT

STAINLESS BOLTS

NON-MAGNETIC END

Figure 11

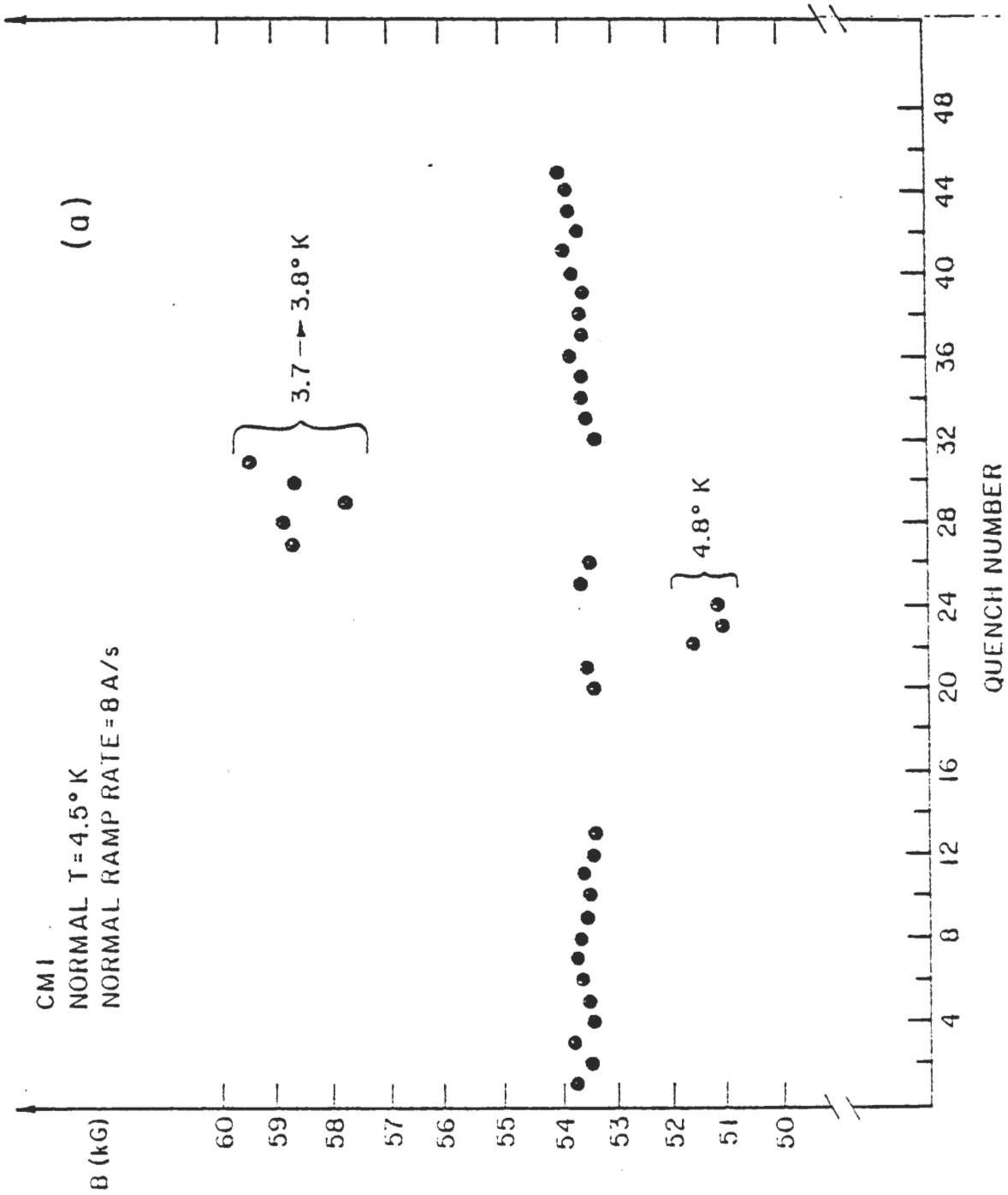


Figure 12a

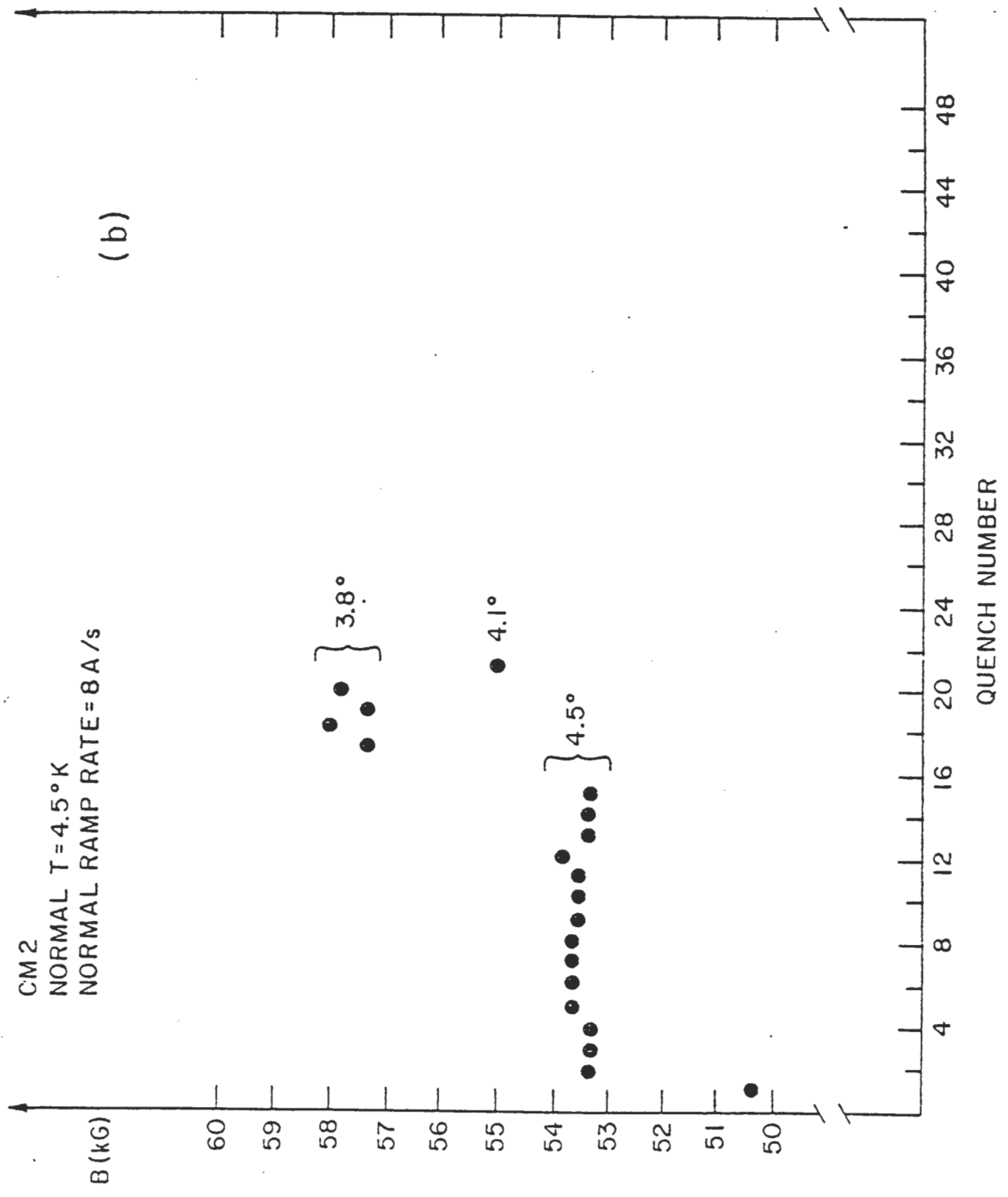


Figure 12b

● DATA
○ EXTRAPOLATION

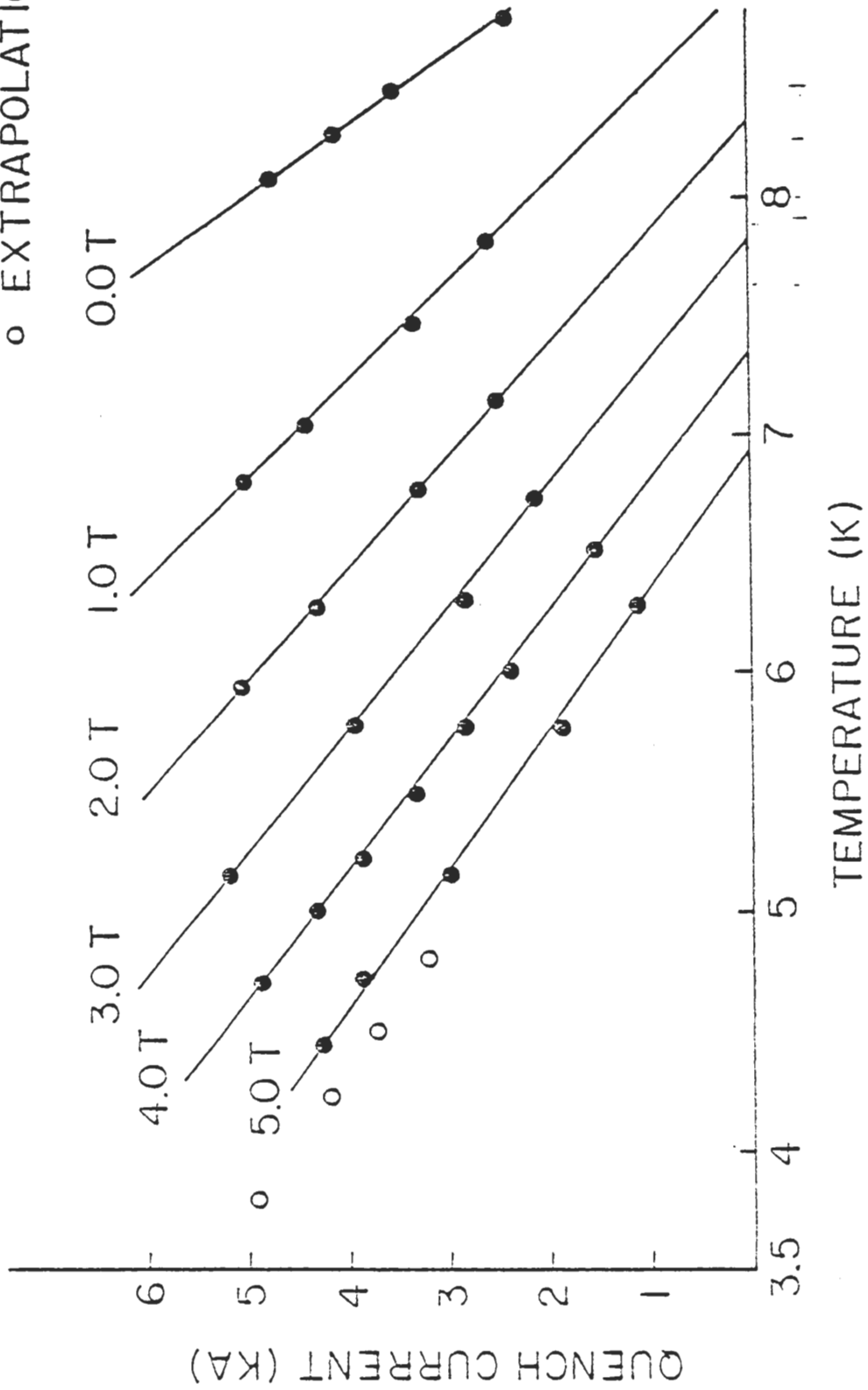


Figure 13

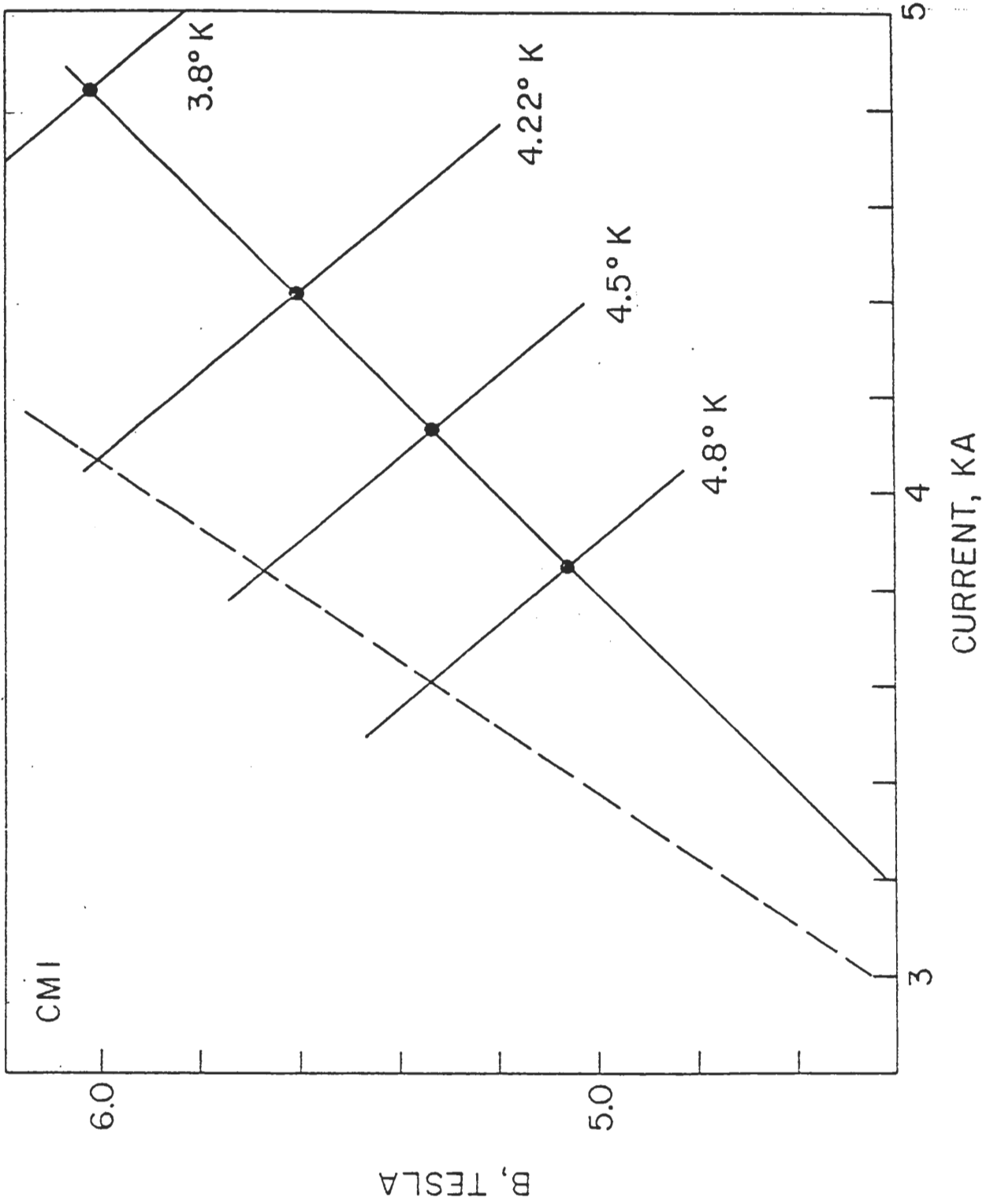


Figure 14

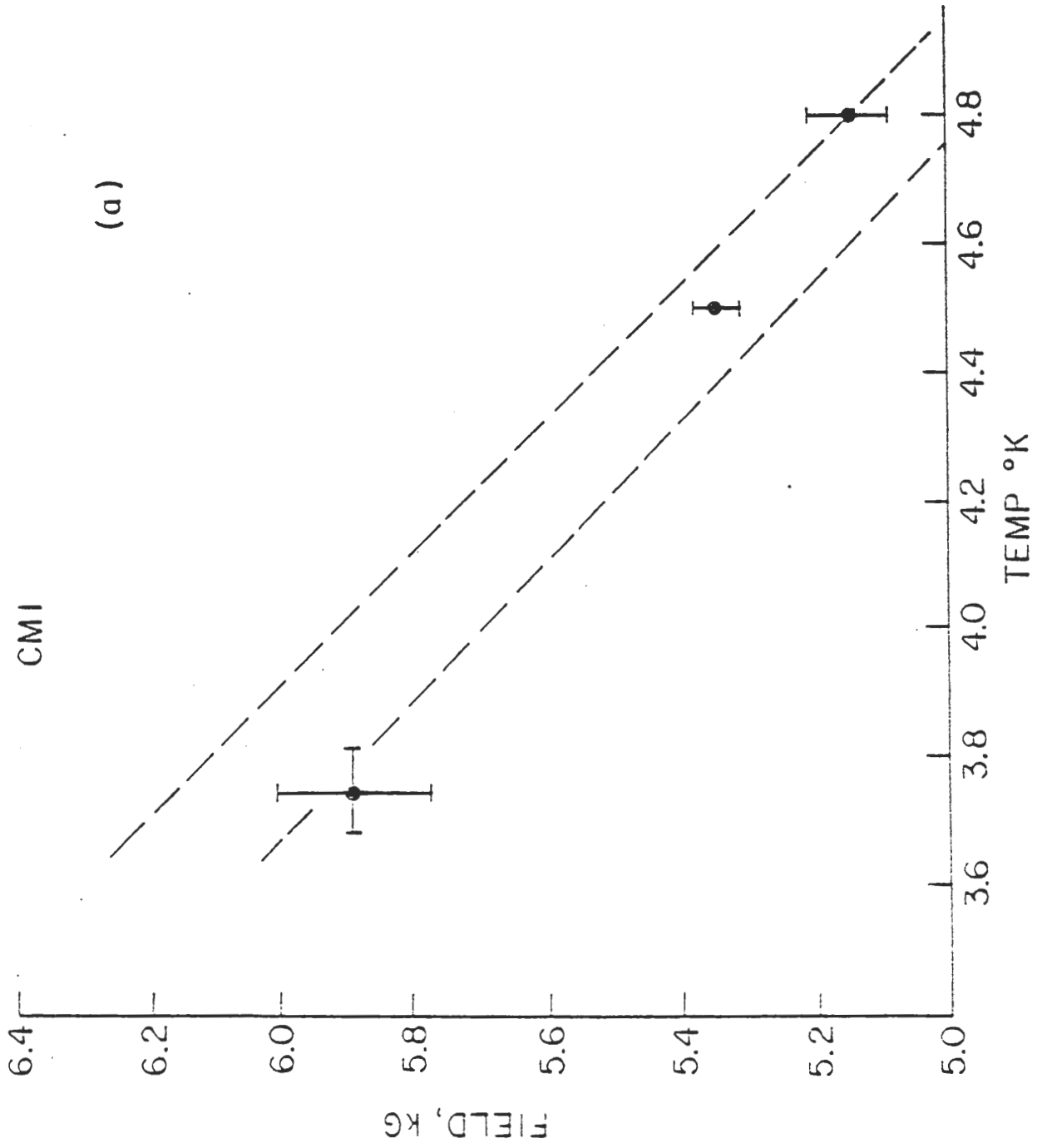


Figure 15a

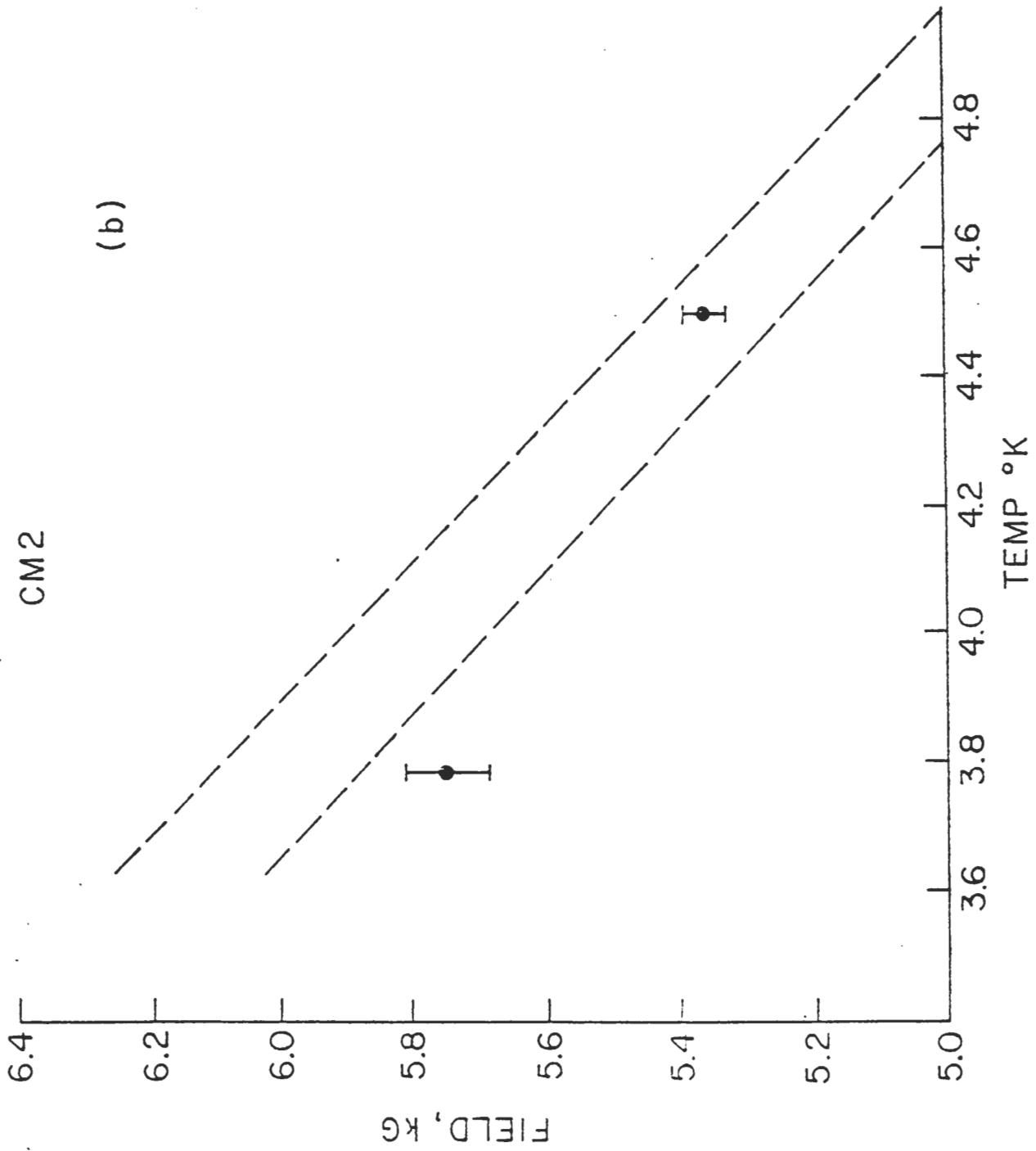


Figure 15b

MAGNETIZATION
 b_2' vs. I

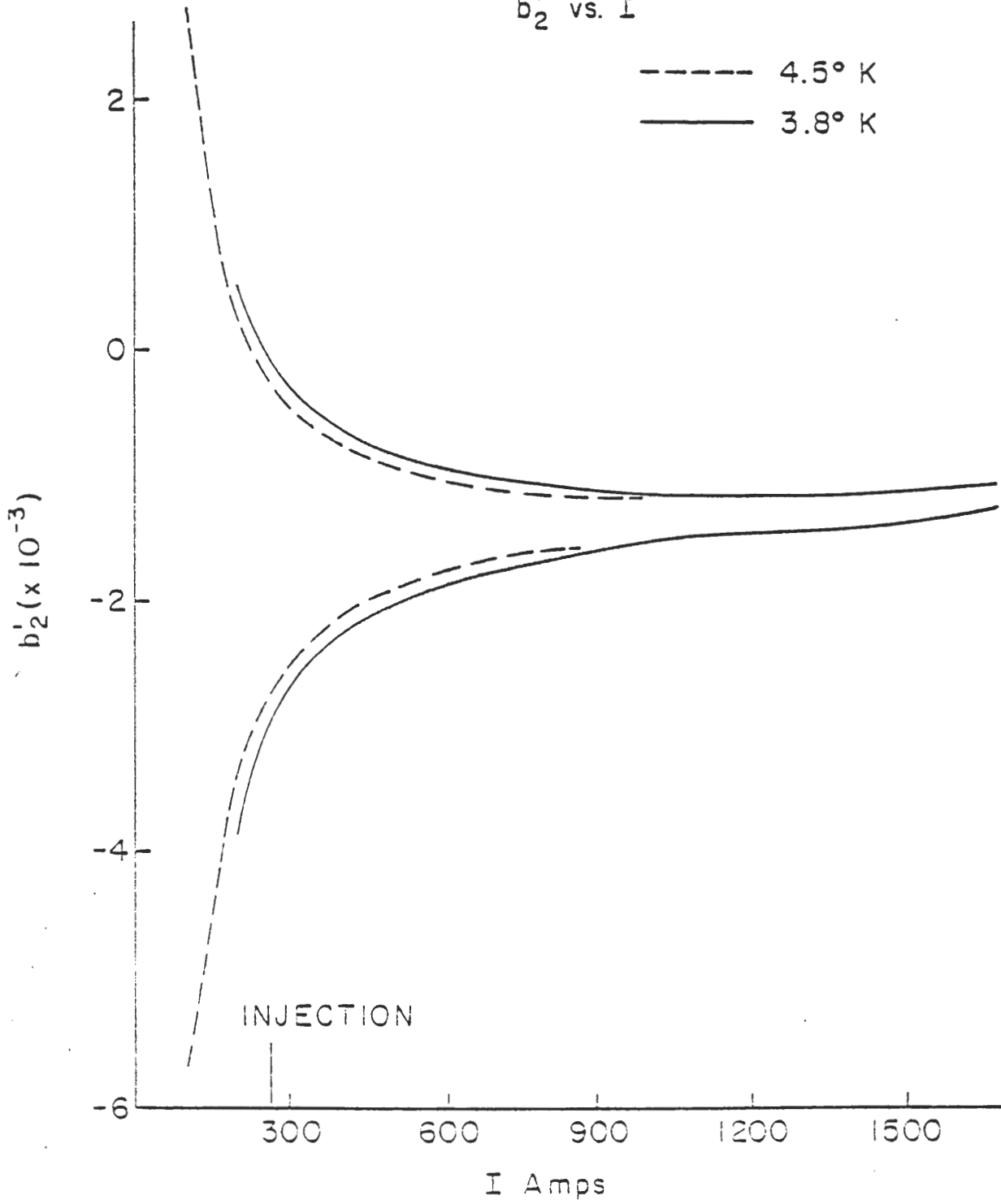


Figure 16

B TESLA

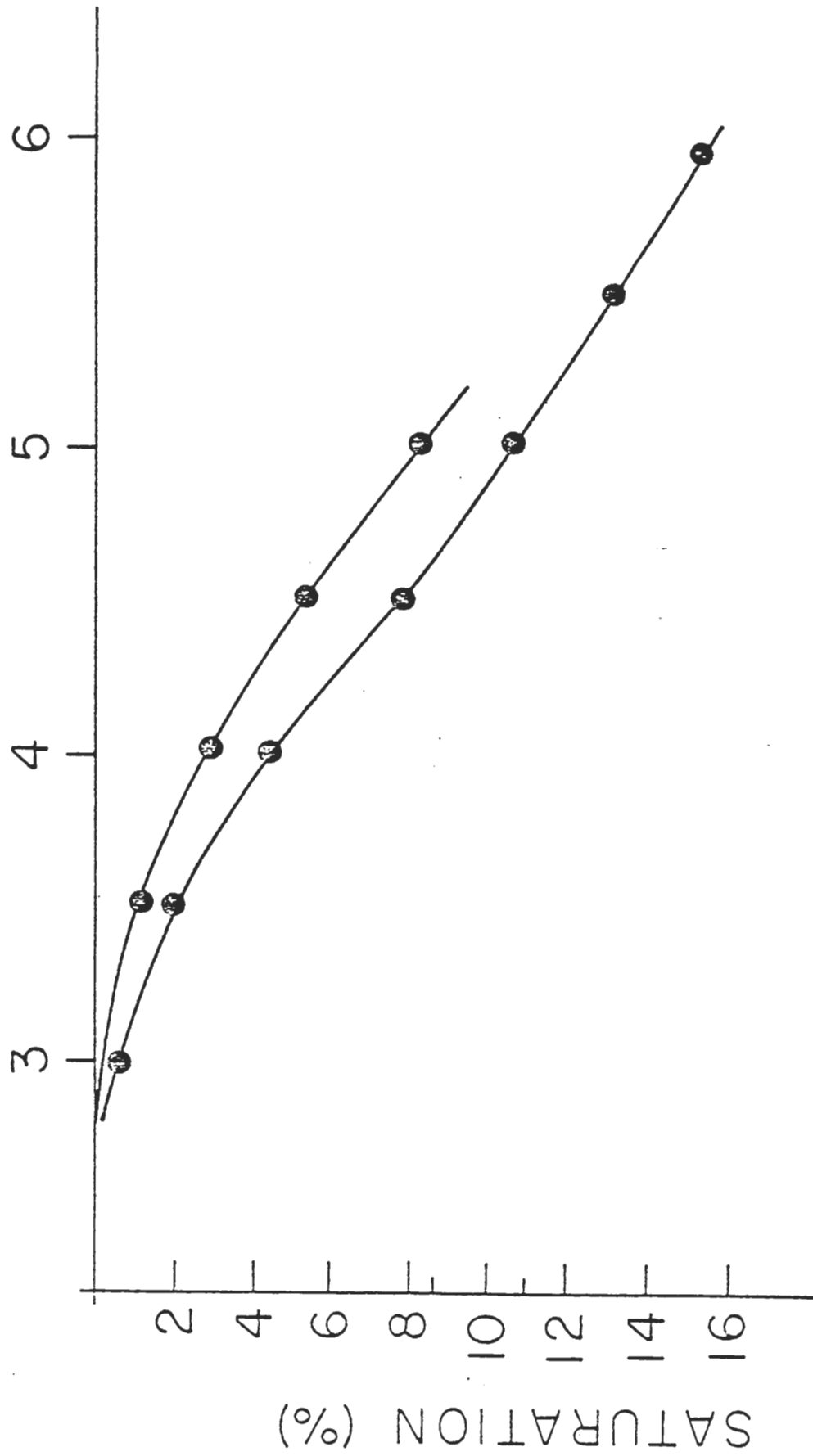


Figure 17

b_2' and b_4' vs. I for CMI

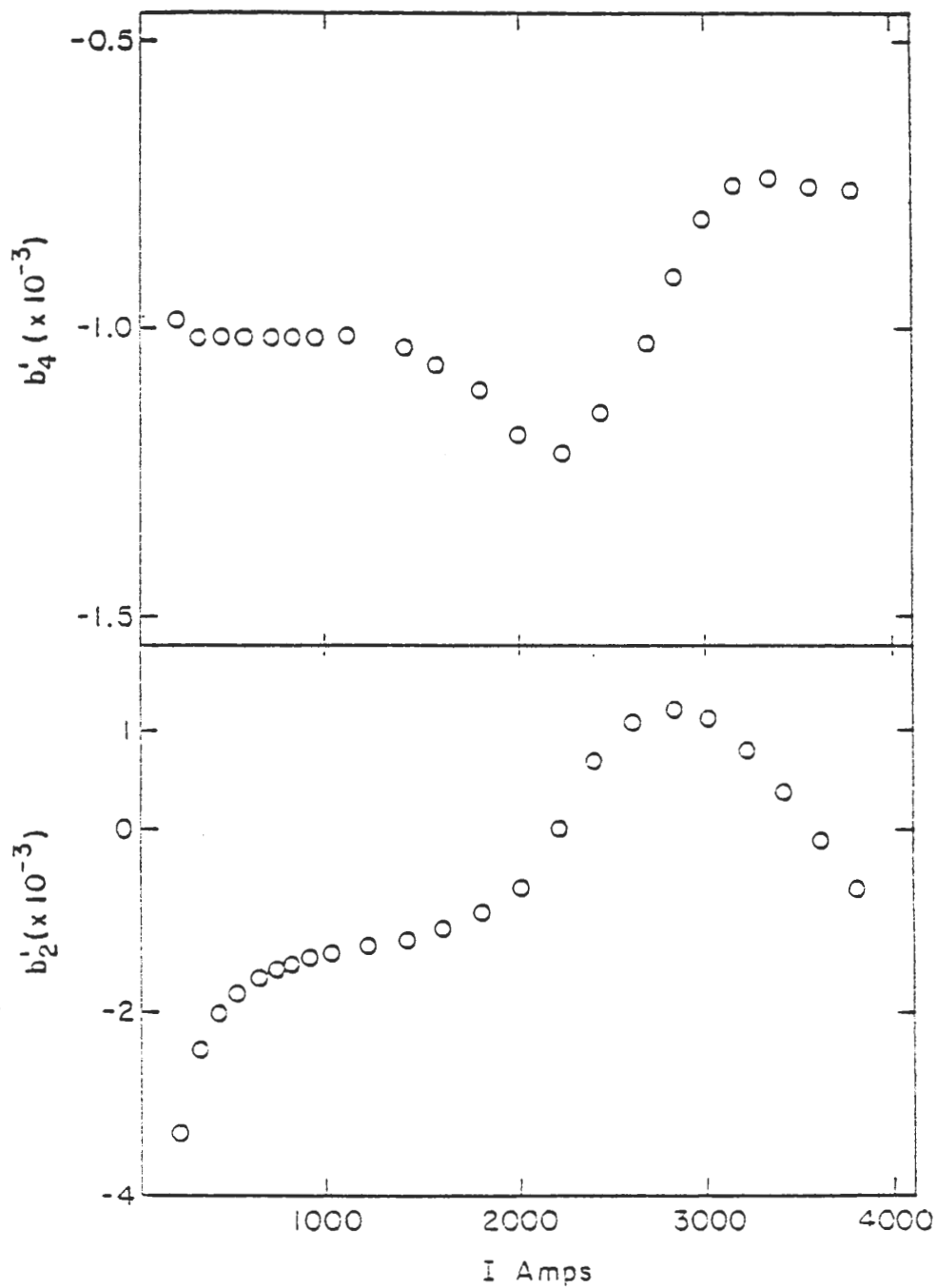


Figure 18

Distribution:

ISABELLE Project S&P

902-C - 20 copies

I. Montanez
H. McChesney
F. Ascolese
J. Kind

Bldg. 911

G. Danby
H. Fadem
S. Ghoshroy
J.W. Glenn
C. Goodzeit
D. Gough
J. Grisoli
J. Jackson
A. Kaam
J. Keohane
D. Lazarus
Y. Lee
D. Lowenstein
Y. Makdisi
P. Montemurro
R. Nawrocky
M. Smith (1) plus one
for each author(s) file
R. Thorn
J. Tuozzolo
W.T. Weng
P.B. Zuhoski
K. Kohler

Bldg. 725

K. Batchelor
E. Bozoki
J. Dickerson
J. Galayda
S. Krinsky
J. Sheehan
A. Luccio

W.R. Casey, 535A
D.G. Dimmler, 535
J. Neiderer, 515

Bldg. 510

N. Samios
R.P. Shutt
H. Gordon
T.F. Kycia
L. Leipuner
S. Lindenbaum
S. Ozaki
S. Protopopescu
D. Rahm
M. Sakitt
R. Fernow 510-C
I. Stumer
T.L. Trueman

